Letters in Applied NanoBioScience
Platinum Open Access Journal (ISSN: 2284-6808)

Article
Volume 10, Issue 4, 2021, 2655 - 2679
https://doi.org/10.33263/LIANBS104.26552679

Artichoke Extract as an Eco-Friendly Corrosion Inhibitor for Zinc in 1 M Hydrochloric Acid Solution

Hanaa M. Elabbasy [1,*], Omnia A. Mohamed [2], Abd El-Aziz S. Fouda [2]

[1] Misr Higher Institute for Engineering and Technology, Mansoura, Egypt; helabbasy@hotmail.com (H.M.E.);
[2] Department Chemistry, Faculty of Science, Mansoura University, Mansoura-35516, Egypt; asfouda@hotmail.com (A.E-A.S.F.);
* Correspondence: helabbasy@hotmail.com (H.M.E.);

Scopus Author ID 57194688431

Received: 17.01.2021; Revised: 30.03.2021; Accepted: 10.04.2021; Published: 7.05.2021

Abstract: Artichoke extract (AE) was studied as the corrosion inhibitor for zinc in 1 M HCl utilizing chemical and electrochemical methods. The adsorption isotherm of Artichoke extract on Zn surface accords with Langmuir adsorption isotherm. The inhibition efficiency increases with increasing the extract's concentration and decreases with the rise in the medium's temperature. The inhibition efficiency reached a value of 93.2% at 300 ppm of extract. This extract may be forming a film and acts as a barrier, which minimizes the contact area between zinc surface and HCl solution. Artichoke extract acts as a mixed inhibitor in HCl solution. Thermodynamic parameters of activation and adsorption were determined and explained. The adsorption parameters also obeyed the Langmuir adsorption isotherm, and the sign of the free energy of adsorption showed a spontaneous process. The surface morphology of zinc metal was examined by employing various techniques. Also, the biological effect of the Artichoke extract was studied. Theoretical studies of quantum mechanics and molecular dynamics simulations studies were carried out on the Artichoke extract compounds, and the results agree with the experimental one. The efficiencies marked from all employed techniques were in perfect correspondence, demonstrating the validity of these procedures.

Keywords: zinc; artichoke extract; corrosion inhibition; HCl; AFM; biological effect; SEM.

1. Introduction

Zn is a non-ferrous metal used in metallic coating, extensively, a natural metal founds in the earth's crust. Besides rock and soil, present in water, air, and the biosphere, is concluded in plants, animals, and humans. Zinc is a metal with numerous industrial applications and is mainly used for the corrosion protection of steel [1]. Zinc is an industrially important metal and is corroded by many agents, of which aqueous acids are the most dangerous [2]. Zn metal is highly susceptible to attack by acids, especially sulphuric and hydrochloric acids. In the current industry, acids are used for the chemical cleaning of metals and alloys. Thence for scale elimination and cleaning of zinc surfaces by acidic solutions, it is required to use inhibitors [3]. The employment of the plant extracts as inhibitors to lower the dissolution of metals in several typical industrial solutions was performed by several authors [4-18]. Inhibitors from plant extracts are characterized by their renewable resources, facilely obtainable, low cost, and no harmful effects on the environment [19]. The green corrosion extracts mainly contain the needful elements (such as O, C, N, and S) that help molecules to be adsorbed on the surfaces of metals or alloys to form a film that protects the surface from corroded [20]. There is no

indication to apply this extract as a corrosion inhibitor for zinc in HCl solution in the literature survey. This encourages us to utilize this extract as a corrosion inhibitor for zinc in HCl medium. Artichoke extract AE (*Cynara cardunculus* var. *scolymus*) [21], Family: *Asteraceae* [22]. It is an accepted known plant, coming from the Mediterranean Sea, Italy, and Spain. Artichoke consists of apigenin and luteolin bioactive agents [23]. Its leaves are consumed as vegetables worldwide and are applied, for a long time, in herbal medication as a choleretic [24]. Besides polyphenols and flavonoids, some mono- and dicaffeoylquinic acids were found as the main portion in the chemical constituents of artichoke leaves [25].

This research article evaluates the AE as an inhibitor for Zn in a corrosive acid medium by employing several techniques. This included the elucidation of the protection mechanism involved.

2. Materials and Methods

2.1. Materials and plant preparations.

The acid corrosive medium (1 M HCl) was prepared by diluting a reagent of analytical grade HCl 37% with bi-distilled water. The composition of the applied Zn as weight % is Cd (0.52), Fe (0.035), Mn (0.005), Pb (0.18), Sn (0.07), and Zn rest. The Zn sheet of thickness 0.1 cm was mechanically press-cut into 2×2 cm coupons for ML measurements and 1×1 cm for electrochemical measurements. The samples were abraded with varying degrees of emery papers reaching 2000 grades, cleaned and washed using acetone and bi-distilled water, and dry with filter paper. The coupons were then ready to use in the corrosion studies. The freshly Artichoke parts were firstly prepared to dehydrate, milled to a powder. Then, 500 g of the powder drenched in methanol, boiling at 100 °C, and preserved at room temperature for about 72 hours. After that, the AE is filtrated and put in the air to dry. To attain 1000 ppm stock solution of the extract, one-gram from the dried AE is dissolved in one litter bi-distilled water. Various concentrations (from 50 to 300 ppm) are prepared from the AE solution through dilution with bi-distilled water.

2.2. Mass loss (ML) method.

Zn samples with dimensions 2 x 2 x 0.1 cm were utilized in this method. Before all experiments, the samples were mechanically abraded by 800-2000 grades of emery papers, washed by bi-distilled water, degreased with acetone, dried by filter paper, and weighed accurately by employing an analytical balance by 0.1 mg of precision. The samples then suspended in solutions of 100 ml of the corrosive acid medium without and with (50, 100, 150, 200, 250, and 300 ppm) of AE for different immersion time (60, 120, 180, 240, 300, and 360 min), then the samples were taken away and handled following the process cleared in ASTM term G1-90 [26].

2.3. Electrochemical techniques.

For electrochemical procedures, a conventional glass cell of three electrodes was employed. A cylindrical rod working electrode (Zn metal) was placed into a glass tube of appropriate diameter using epoxy resin. It offered an active flat-disc-shaped surface of 1 cm^2 geometric area to contact with the electrolyte, saturated calomel electrode (SCE) as a reference electrode, and auxiliary electrode (Pt), respectively [27]. Before each electrochemical

measurement, the Zn electrode was polished with emery papers and treated as in ML, left for 30 min in the solution to give a chance to the open circuit potential to attain a steady-state [28]. The potentiodynamic polarization (PP) curves were recorded in the potential range of -500 to +500 mV relating to the open circuit potential (E_{ocp}) at a scan rate of 0.5 mV s^{-1}.

Electrochemical impedance spectroscopy (EIS) was recorded at open circuit potential, OCP. The AC signal was 10 mV peak to peak with a frequency range between 50 kHz and 0.1 Hz.

The electrochemical frequency modulation (EFM) procedures employed a potential amplitude of 10 mV, with two sine waves of 2 and 5 Hz. The EFM procedure outcomes are spectra (termed intermodulation spectra) of current response as a function of frequency. The spectra consist of current responses selected for harmonically and intermodulation current peaks. The bigger peaks were employed to attain the corrosion current density (icorr), the causality factors (CF-2 and CF-3), and the Tafel slopes (βc and βa) [29]. The large strength of the EFM is the causality factors that show an internal check on the sincerity of the EFM procedure [30]. For the reproduction of the data, each experiment was repeated at least three times.

Electrochemical techniques were carried out using Potentiostat/ Galvanostat (Gamry PCI 300/4) with software DC105 for polarization, EIS300 for EIS, and EFM140 for EFM, connected to a computer for data record and store. All the experiments were carried out at 25 ^{o}C using an ultra circulating thermostat, and solutions were not deaerated. Each experiment was performed on a newly abraded electrode using a freshly prepared electrolyte.

2.4. Surface analysis.

2.4.1. Scanning electron microscopy (SEM) and energy dispersion X-ray (EDX) analysis.

SEM and EDX analysis of Zn surface before and after immersion for 24 hours in the corrosive acid medium without and with 300 ppm (the higher concentration) of AE were studied using apparatus model: JEOL (Japan JSM IT - 100).

2.4.2. Atomic force microscopy (AFM) analysis.

AFM is an effective method for examining Zn metal's surface morphology at a nano- to micro- scale. The essential feature of this test is that the roughness of the surface can be recorded. AFM tests were carried out using prepared Zn specimens before and after immersion for 24 hours in the corrosive acid medium without and with 300 ppm of AE.

2.4.3. Fourier-transform infrared spectroscopy (FT-IR) studies.

FT-IR spectra were registered in a spectral range 4000 to 500 cm^{-1} with the technique of Attenuated Total Reflectance (ATR) using FTIR-Spectrometer iS 10 (Thermo Fisher Scientific, USA). FT-IR spectrum is an effective way to compare between the inhibitor and corrosion products after inhibitor adsorption. The FT-IR peak values were recorded for AE and for Zn after immersion for 24 hours in the corrosive acid medium containing 300 ppm of AE.

2.4.4. Ultraviolet-visible spectroscopic (UV) test.

The formation of a metal complex is supported mainly by using the Ultraviolet-visible spectroscopic test. The UV absorption spectra of the corrosive acid medium with 300 ppm of

AE were investigated without and after Zn immersion for 24 hours. The UV spectra were carried out using UV spectrometer T80+ (UV TIS model, UK).

2.5. Biological effect.

A biological effect test was carried out for AE to detect multiplying bacteria by determining the number of Bacteria colonies using the Doc-it colony counter instrument.

3. Results and Discussion

3.1. Mass loss (ML) test.

The effect of adding different concentrations (from 50 to 300 ppm) of AE to Zn's corrosive solution was tested using ML. The average ML at a definite time for the Zn samples was taken as follows:

$$\Delta W = W_o - W_1 \quad (1)$$

where W_o and W_1 are the weights of the Zn samples before and after immersion in the acid corrosive medium, respectively. The inhibition efficiency (%IE) of AE and Zn surface coverage (Θ) can be determined as follows:

$$\%IE = \Theta x\ 100 = [1-(\Delta W_{inh} / \Delta W_{free})] \times 100 \quad (2)$$

where ΔW_{inh} and ΔW_{free} are the ML (mg) without and with AE, respectively. The corrosion process rate (C.R) is calculated as follows:

$$C.R. = \Delta W/At \quad (3)$$

where A is the area of specimens in cm^2 and t is the immersion time in min. Figure 1 illustrated the relationship between ML of different AE concentrations and time (in min) at 25 °C.

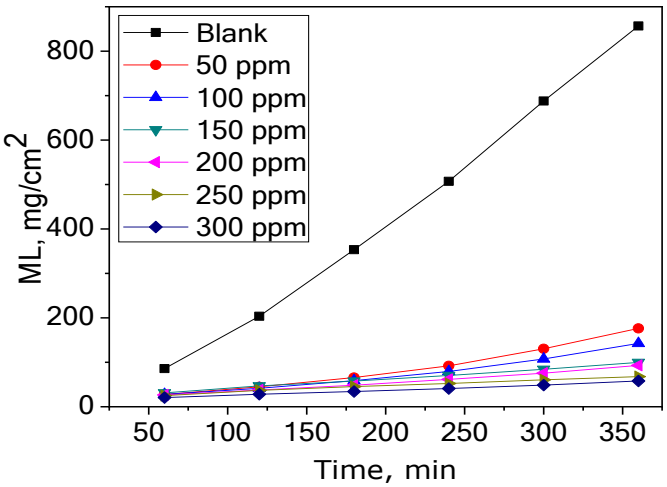

Figure 1. Effect of rising amount of AE on ML at 25 °C for Zn in the corrosive acid medium.

The ML of Zn in the existence of AE was considerably less than that attained in the blank corrosive medium. Meaning that the adsorption of extract molecules on the Zn surface makes a block between the metal and the corrosive acid medium. Hence, the corrosion rate decreases and % IE increases. This indicates that AE behaves as a corrosion inhibitor.

3.1.1. Effect of temperature.

The influence of temperature on C.R. (Figure 2) and on % IE (Figure 3) for Zn in the corrosive acid medium without and with different concentrations of AE was analyzed by ML tests in the temperature range (from 25 to 45 °C). The figures demonstrate that the increase in AE concentration decreases C.R. and increases % IE at all the applied temperatures. This is typically due to the increase of adsorption and coverage of metal surfaces with the raising of AE [31].

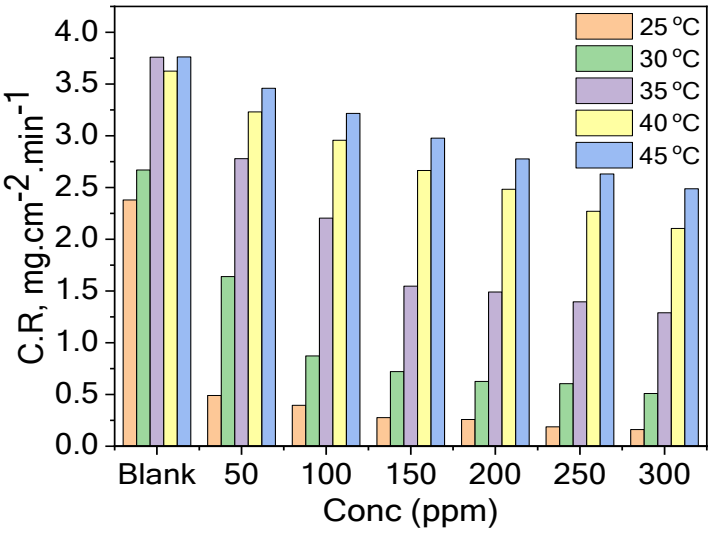

Figure 2. C.R of Zn in the corrosive acid medium vs. concentration of AE at different temperatures.

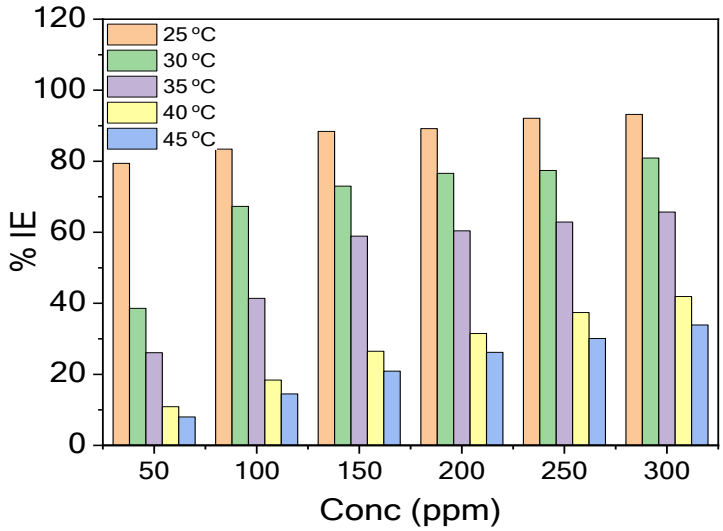

Figure 3. % IE of different AE concentrations for Zn in the corrosive acid medium at different temperatures.

The estimation of activation energies (E_a^*) for corrosion of Zn in uninhibited and inhibited acid corrosive medium were computed by employing the following Arrhenius equation:

$$\log C.R. = - E_a^*/2.303RT + \log A \quad (4)$$

where A is Arrhenius pre-exponential multiplier, T is Kelvin temperature, R is universal gas constant in joule/mol/K unit. Straight lines were obtained by plotting log C.R versus 1/T without and with different AE concentrations (Figure 4) with slope equals ($-E_a^*/2.303$ R). The entropy (ΔS^*) and enthalpy (ΔH^*) of the activation process for Zn in the corrosive acid medium without and with different concentrations of AE were computed by employing the next transition-state equation:

$$C.R = RT/Nh \exp^{(\Delta S^*/R)} \exp^{(-\Delta H^*/RT)} \quad (5)$$

where N & h represents Avogadro's number and Planck's constant, respectively. Straight lines were obtained by plotting log C.R/T versus 1/T without and with different concentrations of AE (Figure 5) with slope equals ($-\Delta H^*/2.303$ R), and the intercept equals [(log (R/Nh) + ($\Delta S^*/2.303$ R))]. The computed activation parameters (E_a^*, ΔH^*, and ΔS^*) were provided in Table 1. The data in Table 1 illustrated that the values of E_a^* in the existence of AE are higher than that in the blank corrosive medium.

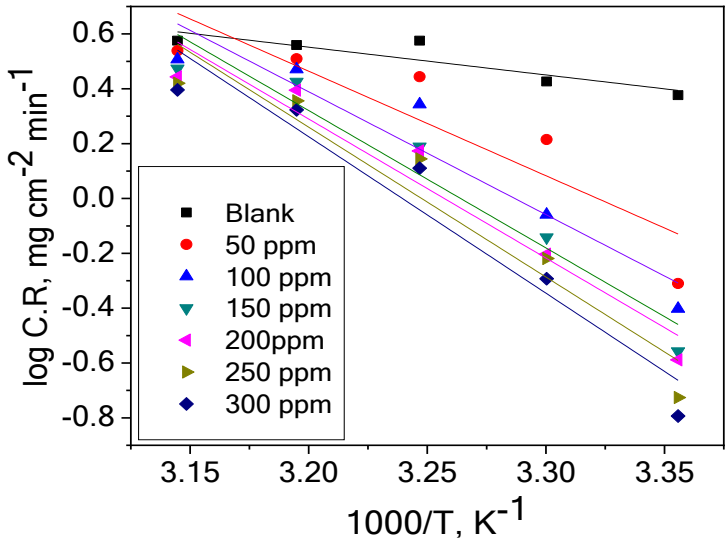

Figure 4. Plotting log C.R. against 1/T for Zn in the acid corrosive medium without and with different AE concentrations.

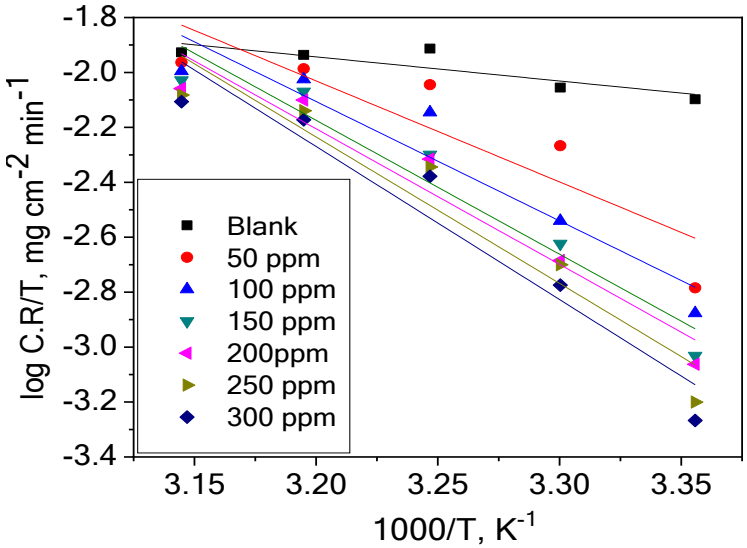

Figure 5. Plotting log C.R/T against 1/T for Zn in the acid corrosive medium without and with different AE concentrations.

The increase in the E_a^* indicates a high adsorption of the AE particles on the Zn surface. As indicated from Table 1, ΔH^* values have positive signs, which means that the AE molecules are adsorbed endothermically on the Zn surface. The increase in ΔH^* in the AE's existence indicates that the energy barrier in the corrosion reaction increases. The mean difference between E_a^* and ΔH^* is about 2.6 kJ mol^{-1}, which is nearly the RT value (2.63 kJ mol^{-1}) [32,33]. This proves that the dissolution of Zn in the corrosive acid medium is a unimolecular reaction. The values of ΔS^* in Table 1 prove that the activated complex in the rate-determining step displays an association instead of dissociation, i.e., the disorder is done on the path of transmitting from reactant to activated complex [34].

Table 1. Activation parameters (E_a^*, ΔH^*, and ΔS^*) for Zn in the corrosive acid medium without different AE concentrations.

C_{inh}, ppm	E_a^*, kJ /mol	ΔH^*, kJ /mol	ΔS^*, J /mol/K
Blank	19.4	16.8	-180.86
50	73.0	70.4	-11.14
100	85.7	83.2	28.30
150	95.9	93.3	59.51
200	97.1	94.5	62.63
250	104.6	102.0	86.16
300	109.2	106.6	100.28

3.1.2. Adsorption study.

To definite the corrosion mechanism, several adsorption isotherms were employed. The obtained data agreement with Langmuir adsorption isotherm, in which the surface part covered by the inhibitor (θ) is related to the inhibitor concentration (C) through the following equation:

$$C/\theta = 1/K_{ads} + C \quad (6)$$

where K_{ads} is to the adsorption equilibrium constant. The plots of Langmuir isotherm at different temperatures were shown in Figure 6. The values of free energy of adsorption (ΔG^o_{ads}) were gotten as follow:

$$\log K_{ads} = 1/55.5 \exp(\Delta G^o_{ads}/2.303RT) \quad (7)$$

Where 55.5 is to the water concentration in (mol/L) at the solution/metal interface. The counted values of K_{ads} and ΔG^o_{ads} were tabulated in Table 2. The negative values of ΔG^o_{ads} signalize that the adsorption process of AE on Zn surface is spontaneous [35]. The obtained lower values for ΔG^o_{ads}, which lie among 20.4 kJ/mol and 12.1 kJ/mol, appear that an electrostatic interaction occurs between AE and Zn surface (physisorption) [36].

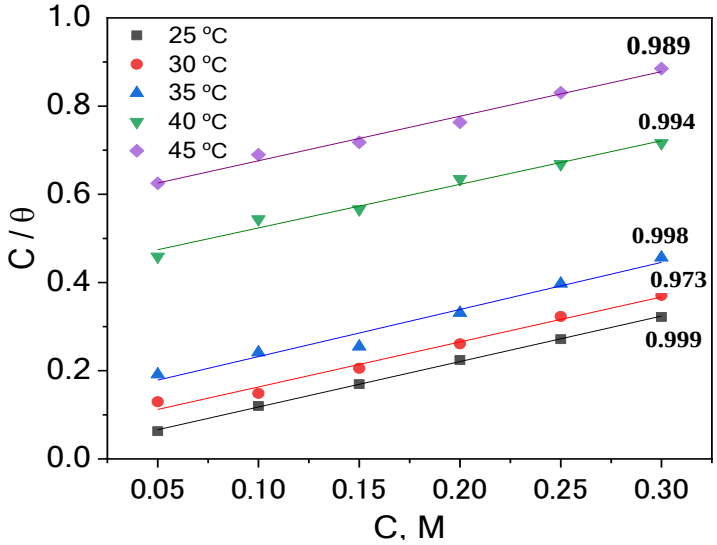

Figure 6. Plots of C/Θ vs. C at different temperatures for Zn in the corrosive acid medium in the presence of AE.

The enthalpy of adsorption (ΔH^o_{ads}) was computed utilizing the following Vant Hoff eq. [37]:

$$\log K_{ads} = -\Delta H^o_{ads}/2.303RT + \text{constant} \quad (8)$$

Plotting log K_{ads} versus 1/T gives a straight line, as shown in Figure 7. The entropy of adsorption (ΔS^{o}_{ads}) can be calculated as follows:

$$\Delta S^{o}_{ads} = (\Delta H^{o}_{ads} - \Delta G^{o}_{ads})/T \quad (9)$$

The calculated ΔH^{o}_{ads} and ΔS^{o}_{ads} values are recorded in Table 2. The negative sign of ΔH^{o}_{ads} points out exothermally adsorption of AE on Zn surface. The calculated values of ΔS^{o}_{ads} point out that an entropy decrease accompanied the process of adsorption.

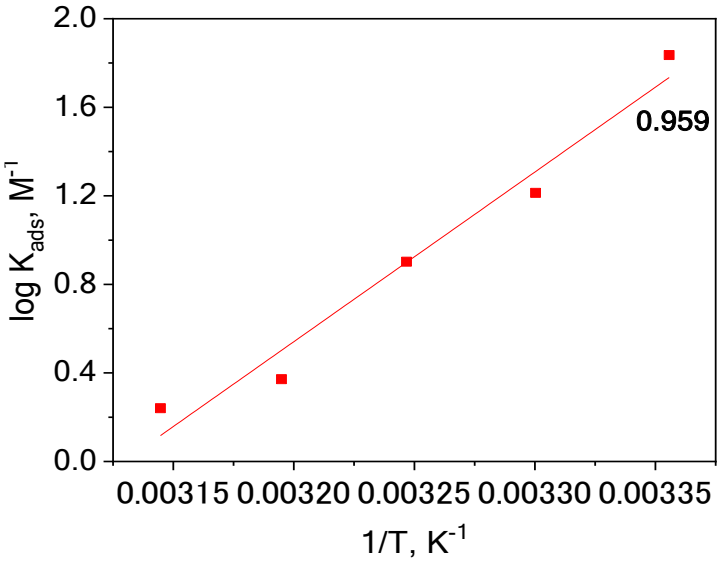

Figure 7. log K_{ads} vs. 1/T for Zn in the corrosive acid medium in the presence of AE.

Table 2. Adsorption parameters for Zn in the corrosive acid medium in the existence of AE at different temperatures.

T, °C	Slope	K_{ads}, M^{-1}	$-\Delta G^{o}_{ads}$, kJ/mol	$-\Delta H_{ads}$, kJ/mol	$-\Delta S_{ads}$, J/mol/K
25	1.031	68.49	20.4		423.8
30	1.020	16.33	17.2		427.4
35	1.068	7.987	15.6	146.7	425.6
40	0.989	2.353	12.7		428.1
45	1.010	1.739	12.1		423.3

3.2. Electrochemical techniques.

3.2.1. Open circuit potential (E_{OC}).

The E_{OC} variation with time for Zn in the corrosive acid medium without and with different concentrations of AE was represented in Figure 8. The inspection of Figure 8 indicates that E_{OC} began from − 964.3 mV for the blank solution and moves progressively to the less negative side (anodically) until attaining the steady-state after 10 min because of the dissolution of the oxide film from the Zn surface. As shown in Figure 8, after adding AE the E_{OC} began at the more negative potential than the blank solution and, after that, moves anodically. The quickly coming off the steady-state, associated with the blank, is because the oxide film's reductive dissolution on the metal surface formed in the air, followed by a new film's growth inside the solution [38]. The initial shifts of E_{OC} when adding different AE concentrations mean that the resistance of Zn dissolution in the corrosive acid medium increases with increasing AE concentration.

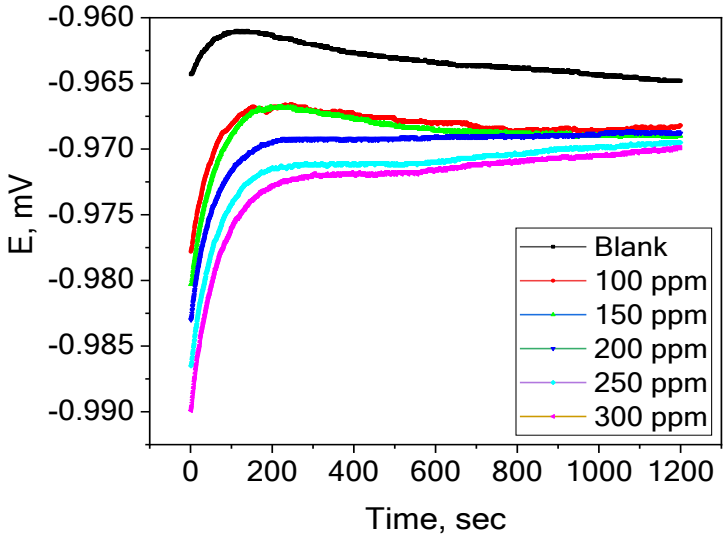

Figure 8. E_{OC} vs. time at 25°C for Zn in the corrosive acid medium without and with different AE concentrations.

3.2.2. Potentiodynamic polarization (PP) test.

Anodic and cathodic curves from the PP test at 25 °C for Zn in the corrosive acid medium without and with different AE concentrations were recorded in Figure 9. The corrosion current density (i_{corr}) was used for calculating (%IE) and (θ) as seen in the next equation [39]:

$$\%IE = \theta \times 100 = [1 - (i_{corr} / i^{o}_{corr})] \times 100 \quad (10)$$

where i_{corr} and i^{o}_{corr} are the corrosion current densities with AE and without it, respectively. Eq. (11) is used to calculate the polarization resistance (R_p) [40,41]:

$$R_p = (\beta_c \beta_a)/[2.303\, i_{corr} (\beta_c + \beta_a)] \quad (11)$$

The corrosion parameters from PP measurements were tabulated in Table 3.

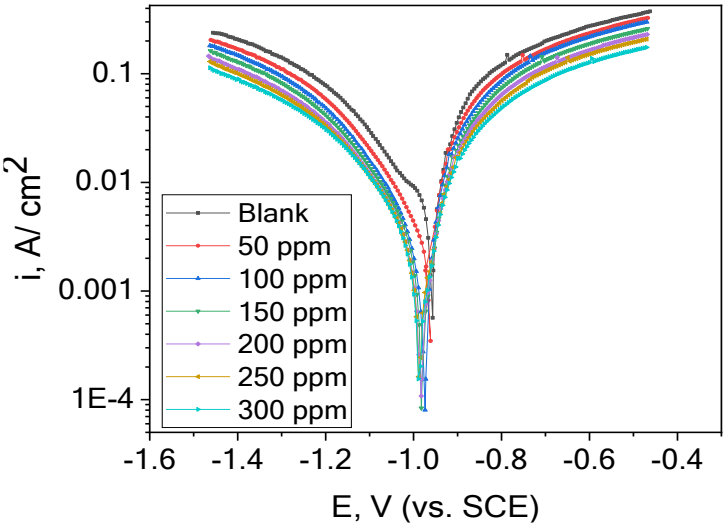

Figure 9. PP curves (anodic and cathodic) for Zn in the corrosive acid medium without and with different AE concentrations at 25 °C.

It is clear from Table 3 that the cathodic and anodic Tafel slopes (β_c & β_a) have a little shift compared to the blank corrosive medium, which means that AE can influence both cathodic and anodic reactions by forming a protective film on the metal surface. The slight change in β_c and β_c values shows no change in the inhibition mechanism in the inhibitor's absence and existence [42,43]. As seen from Table 3, the corrosion potential (Ecorr) value change after adding the AE is fewer than 85 mV that again proves mixed-type inhibition

[44,45]. Table 3 indicates that corrosion current density (icorr) values are lower for inhibited solutions than uninhibited one, and the decrease increasing with the increase in the AE concentration, indicating that AE is a good inhibitor for Zn corrosion in acid media.

Table 3. Electrochemical parameters calculated using PP procedures for Zn in the acid corrosive medium without and with different AE concentrations at 25 °C.

C_{inh}, ppm	$-E_{OCP}$, mV	$-E_{corr}$, mV vs SCE	i_{corr}, mA/cm^2	$-\beta_c$, mV/dec	β_a, mV/dec	R_p Ohm cm^2	C.R mm/yr	$\chi 2$	%IE
Blank	962.4	959	10.70	298	126	3.59	6296	-----	-----
50	967.1	964	4.490	209	93	6.22	2647	0.0050	58.0
100	969.6	974	2.570	162	89	9.73	1518	0.0071	76.0
150	968.0	981	2.090	145	88	11.33	1235	0.0081	80.5
200	968.7	984	1.710	134	85	13.20	1010	0.0089	84.0
250	969.5	986	1.540	108	84	13.29	908.7	0.0090	85.6
300	969.9	987	1.210	93	76	15.04	712.2	0.0054	88.7

3.2.3. Electrochemical impedance spectroscopy (EIS) test.

Nyquist diagrams (without and with fit) and Bode diagrams for Zn in the corrosive acid medium without and with different AE concentrations at 25 °C were shown in Figure 10a without fitting and Figure 10b with fitting and Figure 11, respectively. % IE and θ from EIS measurements were calculated as shown below:

$$\%IE = \theta \times 100 = [1 - (R^o_{ct}/ R_{ct})] \times 100 \qquad (12)$$

where R_{ct} and R^o_{ct} represent the charge-transfer resistance with AE and without it, respectively. EIS parameters are given in Table 4. The equivalent circuit utilized to appropriate the EIS values was given in Figure 12. This circuit consists of stationary phase elements (CPE) rather than capacitors to give many heterogeneity types for corrosion electrodes. The Nyquist plots (Figure 10(a, b)) with and without AE contains a lone capacitive loop signifying the charge transport technique that is extra confirming by single maxima in the corresponding Bode plots. Nyquist plots showed that the semicircle diameter increases with the rise in the concentration of AE. Subsequently, the charge transfer impedance is grown by the corrosion reaction. Nyquist plots' semi-circular shape proves that the process of charge transfer essentially controls the corrosion of Zn [46,47]. The formed AE film on the Zn surface minimizes the double-layer capacitance (C_{dl}) and increases the charge transfer resistance (R_{ct}). The impedance of a CPE is clarified by the next equation [48]:

$$Z_{CPE} = Y_0^{-1}(j\omega)^{n-1} \qquad (13)$$

where Y_0 indicates the CPE quantity and ω indicates the angular frequency of the maximum impedance for the imaginary component, and n is the phase shift, which demonstrations information about the surface inhomogeneity, and j indicates the imaginary number. Higher n indicates minor surface roughness and vice versa. For n = 0 represents the resistance, n =1 represents the capacitance, n = -1 represents the inductance and n = 0.5 represents the Warburg impedance. In the current study, the values of n with and without the extracted molecule is between 0.918 and 0.974. The shift from unity (ideal performance) indicates surface inhomogeneity and surface roughness [49]. The C_{dl} for a circuit involving CPE parameters (Y_0 and n) were determined using the next eq. [50]:

$$C_{dl} = Y_0 (\omega_{max})^{n-1} \quad (14)$$

The parameter ω_{max} is express to $2\pi f$, where f is the frequency of AC. As clear from Table 5, adding different AE concentrations decreases the double layer's capacitance compared to the blank solution. The decrease in the local dielectric constant is because of the replacement of water molecules by the inhibitor [51] and/or the rise in the thickness of the electrical double layer due to the adsorption of extract molecules in the Zn interface/ solution [52]. Bode plots can also sustain the improved surface smoothness in the existence of extract.

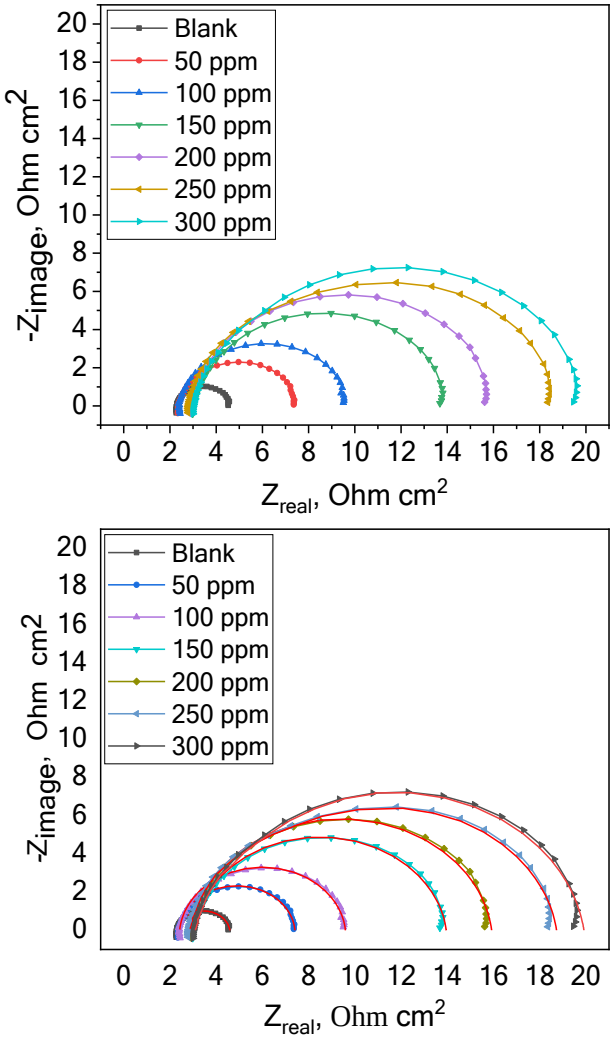

(a) **(b)**

Figure 10. The Nyquist plots (**a**) without fitting; (**b**) with fitting for Zn in the corrosive acid medium without and with different AE concentrations at 25 ºC.

The idealistic capacitor is distinguished by a fixed value of -1 and a phase angle of 90º. This deviancy from the previous data is due to the surface roughness. The deviancy from ideal capacitive behavior is more effective in the absence of extract, as seen from Bode plots. The slope and phase angle values are greatly improved in the presence of extract due to the formation of the defensive layer. The phase angle values are more effective at higher extract concentrations [53]. Low values of the goodness of fit ($\chi 2$) signalize that the fitted data and the experimental data are in high agreement.

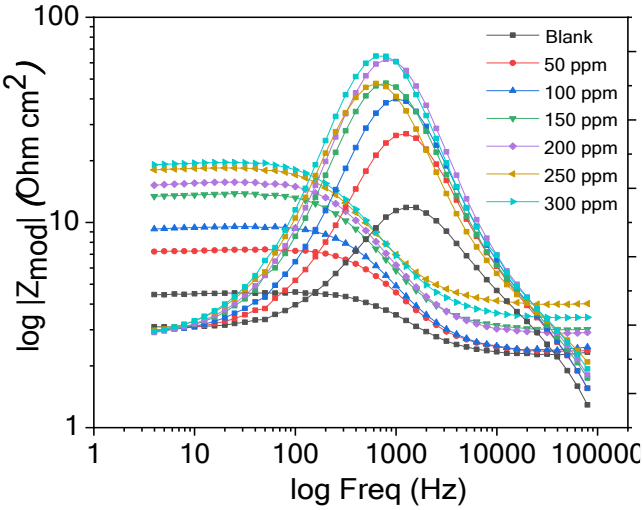

Figure 11. The Bode plots for Zn in the corrosive acid medium without and with different AE concentrations at 25 °C.

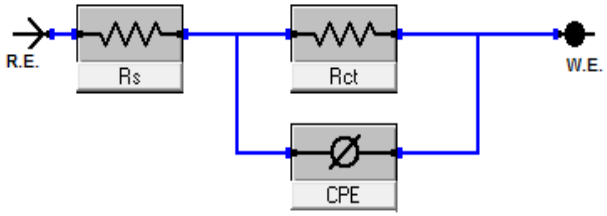

Figure 12. The employed equivalent circuit for appropriate the EIS values.

Table 4. The parameters gained from EIS procedures for Zn in the corrosive acid medium without and with different AE concentrations at 25 °C.

C_{inh}, ppm	R_{ct}, Ohm cm^2	R_u,x 10^3 Ohm cm^2	Y_0, μS^n/Ohm cm^2	N	C_{dl}, μF /cm^2	Θ	%IE
Blank	2.223±0.054	2.304±0.020	93.51±18.4	0.974±0.022	74.84	------	------
50	5.024±0.069	2.384±0.019	70.98±7.9	0.954±0.013	48.24	0.558	55.8
100	7.172±0.090	2.419±0.019	67.98±6.2	0.948±0.010	44.78	0.690	69.0
150	10.93±0.139	3.030±0.024	65.78±5.8	0.929±0.010	40.97	0.797	79.7
200	13.01±0.157	2.916±0.023	61.50±4.6	0.931±0.009	36.16	0.829	82.9
250	14.71±0.188	4.021±0.031	60.62±5.7	0.916±0.010	38.29	0.849	84.9
300	16.46±0.196	3.459±0.027	58.93±4.5	0.918±0.008	34.65	0.865	86.5

3.2.4. Electrochemical frequency modulation (EFM).

Intermodulation spectra of Zn in the corrosive acid medium without and with different AE concentrations at 25 °C were displayed in Figure 13. The more prominent peaks were utilized to compute i_{corr}, β_c, β_a, and the causality factors (CF-2, CF-3). %IE and θ can be calculated from EFM measurements as illustrated in eq. (10). Parameters gotten from EFM procedures were recorded in Table 5. The decrease in i_{corr} with the increase in AE concentration decreases C.R. and increases in Θ, %IE. The closest of CF-2 and CF-3 from theoretical values (2.0 and 3.0) reinforce the validity of Tafel slopes and i_{corr}; this accords with the EFM theory [54,55].

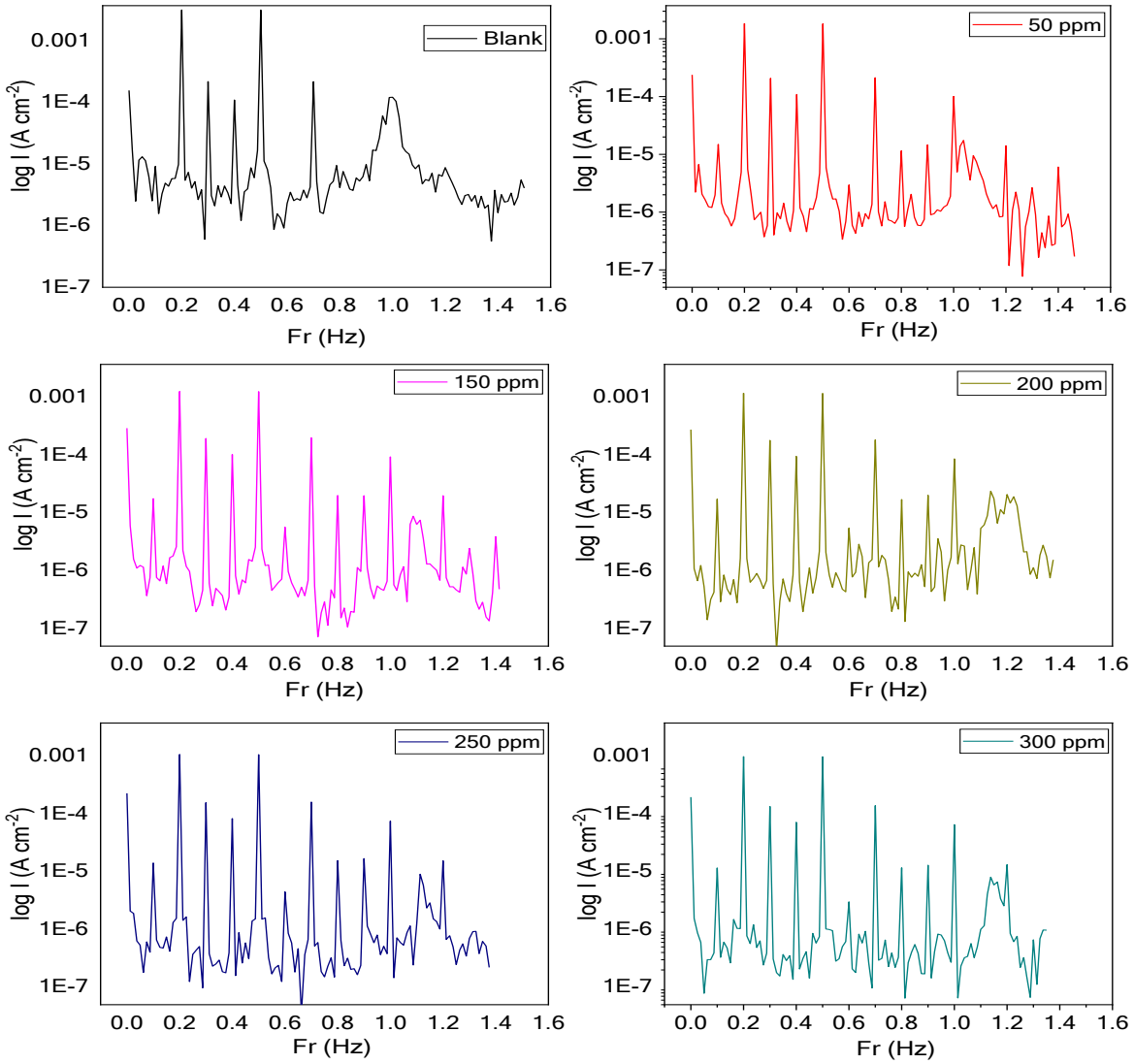

Figure 13. EFM spectra for Zn in the corrosive acid medium without and with different AE concentrations at 25 °C.

Table 5. The parameters gained from EFM procedures for Zn in the corrosive acid medium without and with different AE concentrations at 25 °C.

C_{inh}, ppm	i_{corr}, mA/cm^2	$-\beta_c$, mV /dec	β_a, mV /dec	C.R, mpy	CF-2	CF-3	Θ	%IE
Blank	20.70	394	224	23030	1.884	2.806	--------	-------
50	6.335	111	126	7051	2.000	3.026	0.694	69.4
100	5.189	188	108	5775	2.009	3.160	0.749	74.9
150	2.842	484	86	3163	2.007	2.988	0.863	86.3
200	2.485	393	83	2765	2.004	3.036	0.880	88.0
250	2.385	433	87	2654	2.002	3.234	0.885	88.5
300	2.339	496	94	2607	2.002	3.056	0.887	88.7

3.3. Surface examination.

3.3.1. Scanning electron microscopy (SEM) examination.

The SEM image of Zn sample before exposure to the corrosive acid medium was shown in Figure 14(a). Figure 14(b, c) shows the SEM images for Zn surface after exposure to the corrosive acid medium without and with 300 ppm of AE, respectively. It is shown from Figure 14(b) that the Zn surface was suffering from a severe corrosion attack caused by the corrosive acid medium. The morphology of Zn surface in the presence of AE (Figure 14(c)) indicates a

smoother surface and a change in thickness. This is because of the AE molecules' adsorption on the surface and the formation of a protective film dispersed randomly on the Zn surface, leading to lowering the contact between the metal and the corrosive medium, thus protecting the surface against corrosion [56].

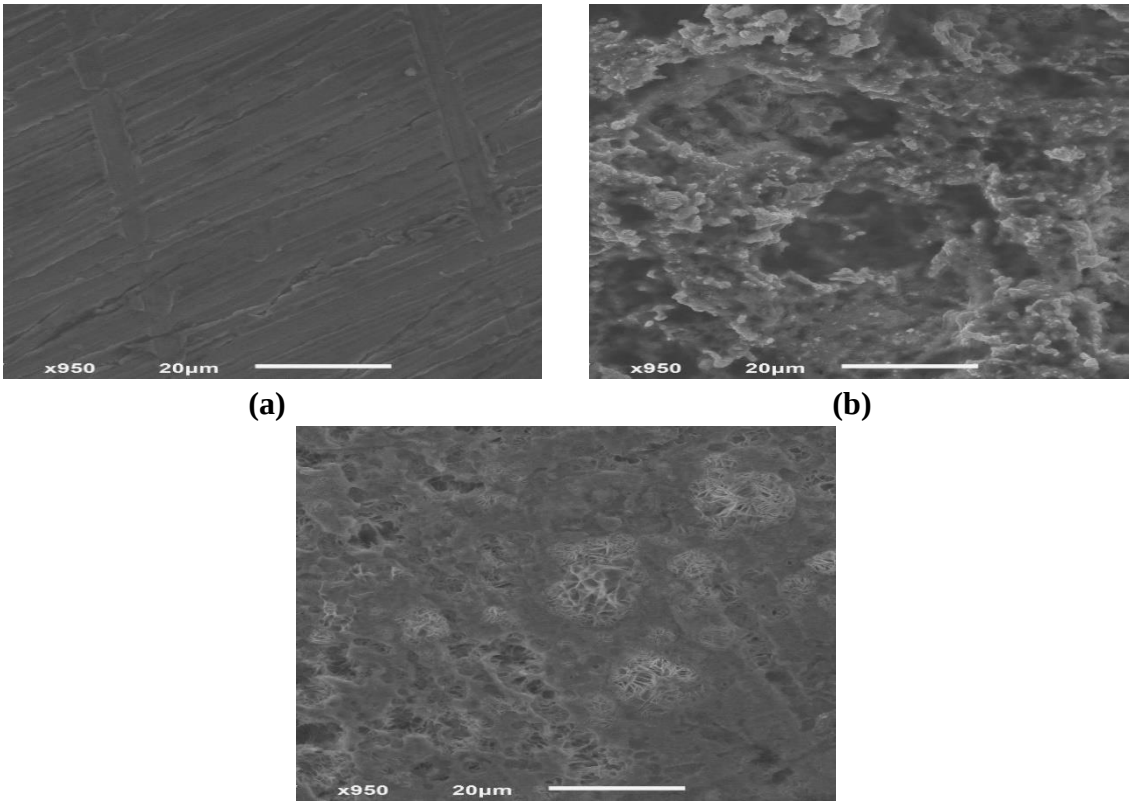

Figure 14. SEM micrographs of (**a**) free Zn; (**b**) Zn after 24 hrs. of exposure to the acid corrosive medium only, and (**c**) Zn after 24 hrs. of exposure to the corrosive acid medium with 300 ppm of AE.

3.3.2. Energy dispersion X-ray (EDX) analysis.

The EDX spectra of free Zn was shown in Figure 15(a). There is O on the Zn surface that indicates the formation of a passive film of ZnO on the surface. Figure 15(b, c) shows the EDX spectra for Zn surface after exposure to the corrosive acid medium without and with 300 ppm of AE, respectively. For blank (Figure 15(b)), the spectra demonstrated the existence of C, O, Cd, Pb, and Cl (gained from HCl medium). The spectra of the inhibited surface (Figure 15(c)) indicate the presence of O, and C (owing to the carbon atoms of AE). The mass percent of elements present in the spectra were recorded in Table 6.

Table 6. Surface composition (mass %) of Zn before and after 24 hours of exposure to the corrosive acid medium without and with 300 ppm of AE.

(Mass%)	Zn	C	O	Cl	Cd	Pb
Free Zn	87.57	10.14	2.30	---	---	---
Zn in blank	57.18	4.89	19.21	3.17	6.94	8.61
Inhibited Zn surface	73.11	8.59	14.56	3.73	---	---

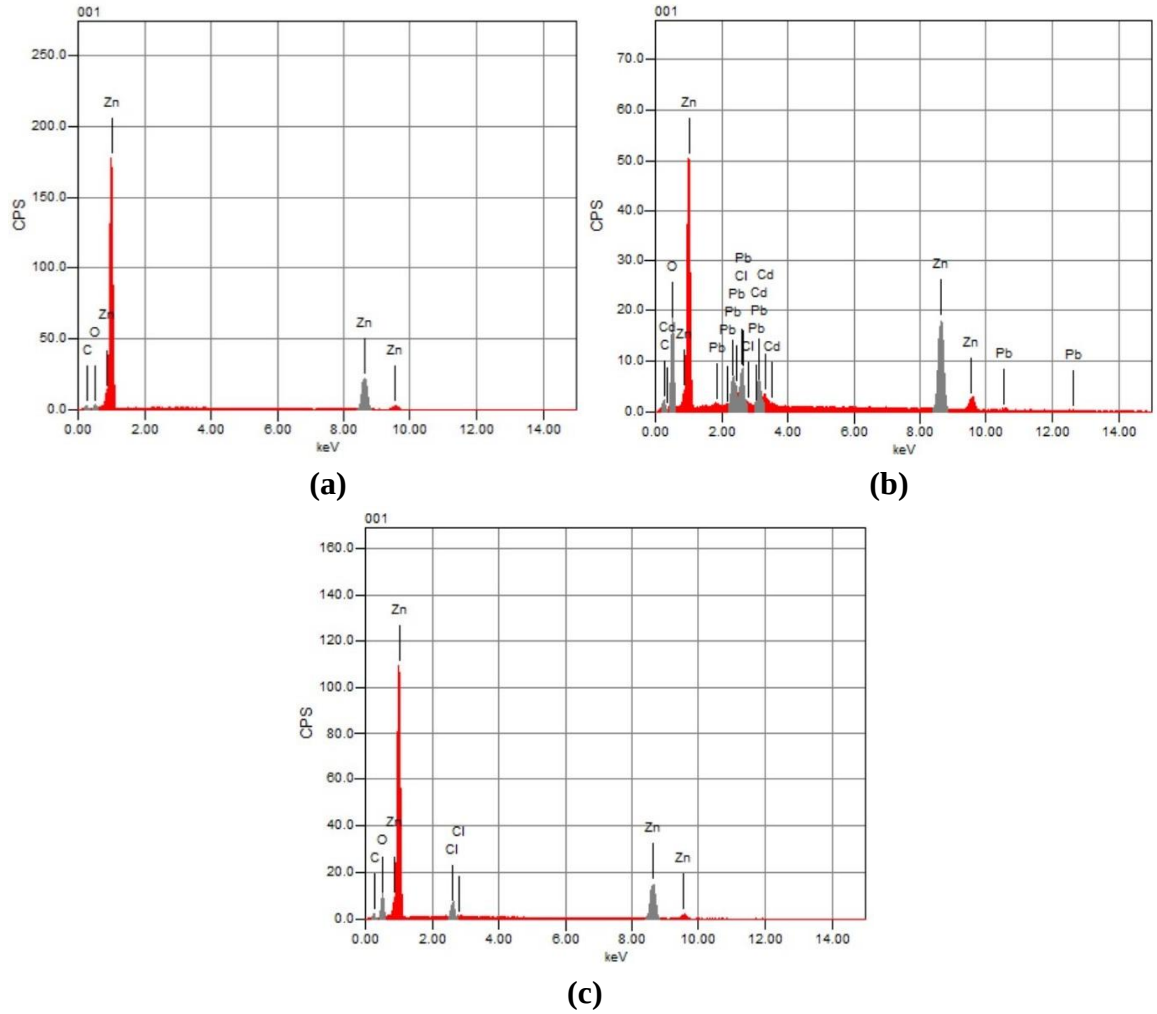

Figure 15. EDX analysis for **(a)** free Zn, **(b)** Zn after 24 hrs. of exposure to the corrosive acid medium only, and **(c)** Zn after 24 hrs. of exposure to the acid corrosive medium with 300 ppm of AE.

3.3.3. Atomic force microscopy (AFM) analysis.

The AFM test is the most important study for analyzing metal surfaces, which is employed to further examine the formed protective film on the surface [57]. Figure 16(a) appears the two –dimensional (2d) and three-dimensional (3d) AFM images of the Zn surface before exposure to acid (free sample). This figure displays the surface of Zn adequately smooth and reflects light. The two –dimensional (2d) and the three-dimensional (3d) AFM images of Zn metal after exposure to acid only (blank sample) and after exposure to the acid with 300 ppm of AE (inhibited sample) are shown in Figure 16(b, c), respectively. Roughness parameters for free, blank and inhibited Zn surface were given in Table 7. The lower roughness was detected on the free sample.

Table 7. Roughness parameters for free, blank and inhibited Zn surface.

Roughness parameters	Free Zn	Zn in blank	inhibited Zn surface
Sa	79.718 nm	617.3 nm	164.76 nm
Sq	99.615 nm	773.68 nm	225.71 nm
Sy	722.38 pm	4.1713 µm	5.7779 µm
Sp	349.42 pm	2071.4 nm	1344.8 nm
Sv	-372.96 pm	-2099.9 nm	-4.433 µm
Sm	-20.019 pm	-10.455 fm	-9.686 fm

The height and roughness of the metal with the extract are less than the blank sample's height and roughness. As the roughness decreases, the inhibitor inhibits corrosion in a higher percent [58]. The lower value of roughness for inhibited solution than uninhibited one is because the adsorption of the inhibitor on the metal surface helps for its protection from getting corroded [59].

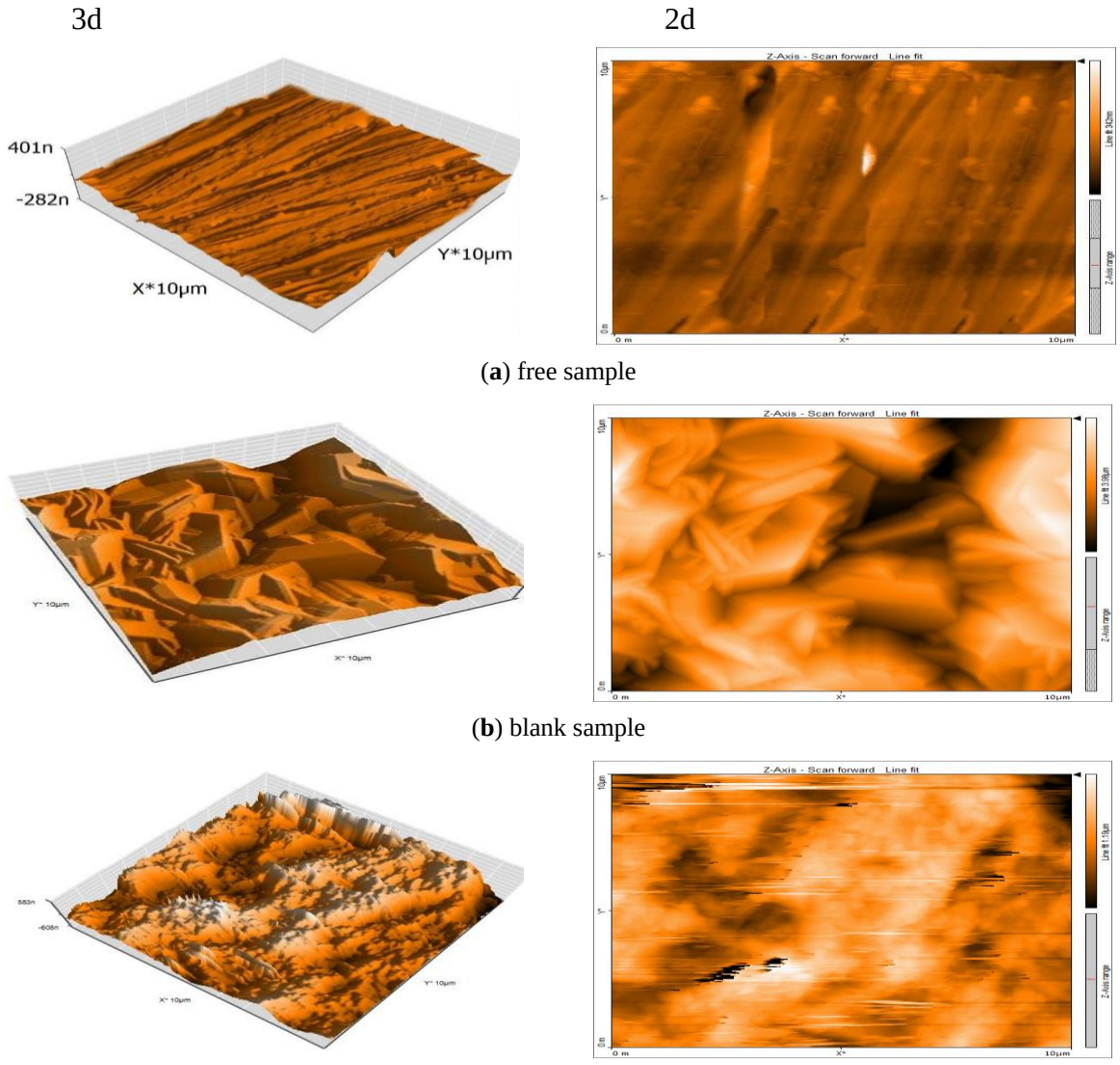

Figure 16. Thethree–dimensional (3d) and the two -dimensional (2d) AFM images of (**a**) free sample; (**b**) blank sample; (**c**) inhibited sample.

3.3.4. Fourier-transform infrared spectroscopy (FT-IR).

The FT-IR spectrophotometer is a useful instrument employed to recognize the functional groups present in the extract and the type of interaction between the function group and metal surface [60]. Figure 17 displays broad peaks of AE at (3331, 2973, 1670, 1381, 1088, and 880 cm^{-1}), which correspond to O-H, carboxylic acid O–H stretching vibration, C=O, C-H, C-O, aromatic C–H bending vibration, respectively. It is clear that there is some peaks displacement between the spectra of the AE and the adsorbed extract from the Zn surface after corrosion. Also, a few peaks are either disappearing or becoming less eminent [61]. This indicates the interaction of AE with Zn through the functional groups present in AE molecules, resulting in the inhibition process.

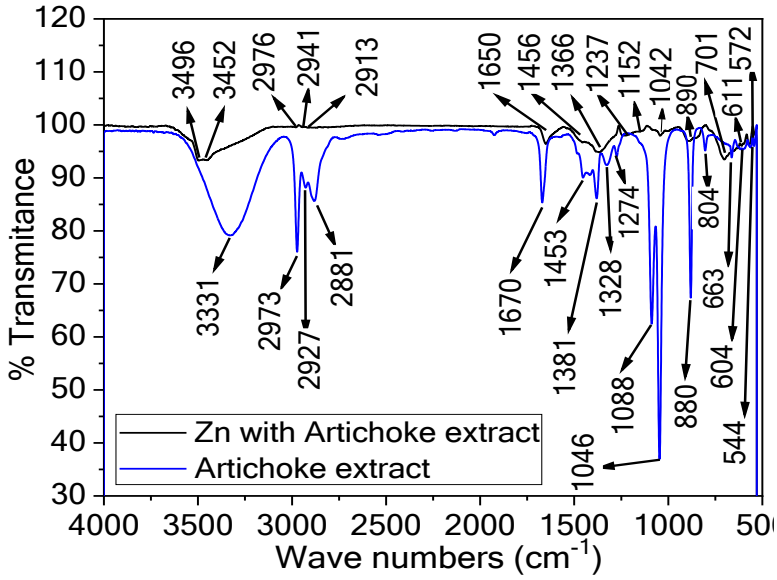

Figure 17. FT-IR spectra for AE and for Zn metal after immersion in the inhibited acid corrosive medium.

3.3.5. UV spectroscopy.

UV–visible spectroscopic checking can be employed to affirm the prospect of complex formation between metal and inhibitor.

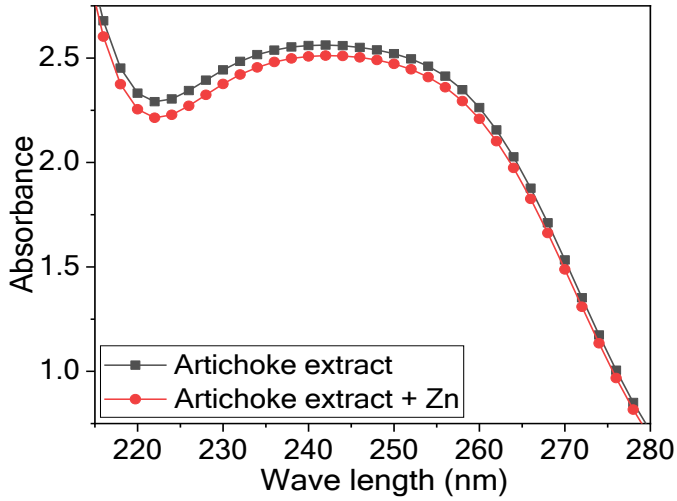

Figure 18. UV–visible absorption spectra of inhibited acid corrosive medium without and with Zn immersion.

The spectra of UV–visible absorption for the corrosive acid medium with 300 ppm of AE without and with Zn immersion are seen in Figure 18. There is a shift in absorbance after Zn immersion. This reveals the formation of a complex between AE and Zn that is responsible for the inhibition activity. Generally, the alteration in the maximum absorbance position and the absorbance value denotes forming a complex between within solution between two species [62]. The shape of the spectra with Zn and without its immersion has no significant variation. It indicates the physical adsorption of the AE on the Zn surface.

3.4. Biological effect.

The biological effect of acute toxicity tests was done for artichoke extract using the Doc-it colony instrument. Original photos of bacteria colonies and the photos using the instrument, for blank and AE, were demonstrated in Figure 19. The number of bacteria colonies cultivated obtained using the Doc-it colony instrument was shown in Table 8. The results of

Table 8 show that the number of bacteria colonies for AE (88 colonies) was lesser than the blank (287 colonies), meaning that AE has a kindly impact in preventing multiplying bacteria, and so the CR decreased.

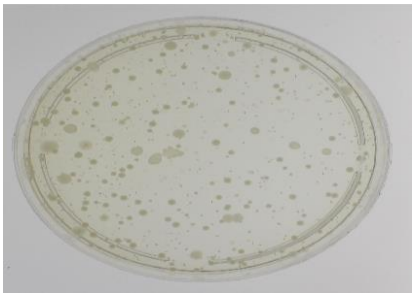

(a_1) original photo for blank

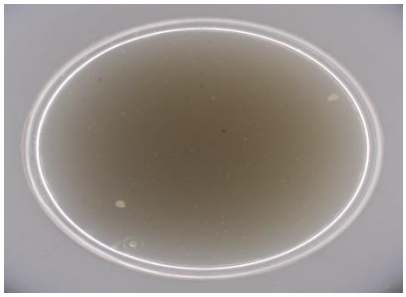

(a_2) original photo for AE

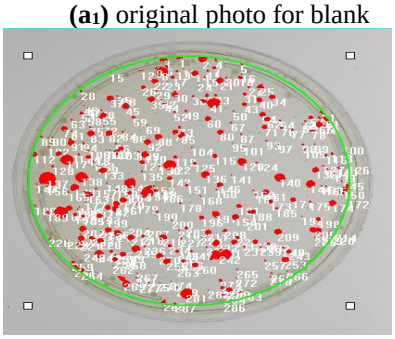

(b_1) photo by Doc-it instrument for blank

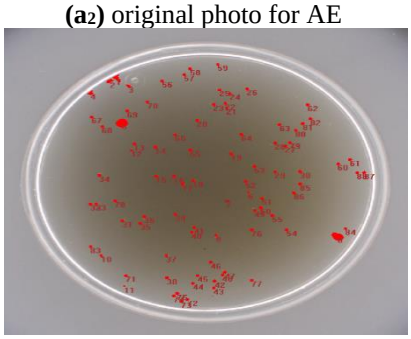

(b_2) photo by Doc-it instrument for AE

Figure 19. Original photos of bacteria colonies for (**a_1**) blank; (**a_2**) AE; photos by Doc-it colony instrument for (**b_1**) blank; (**b_2**) AE.

Table 8. Number of bacteria colonies for blank and for AE as obtained using Doc-it colony counter instrument.

Sample	No of bacteria colonies
Blank	287
AE	88

3.5. Quantum mechanics and molecular dynamics simulations studies.

3.5.1. Quantum mechanics.

The plant extract contains many compounds in low ratios. But, there are two major compounds, they are Apigenin and Luteolin. Their chemical composition as shown in Table 9. Figure 20 shows the optimum geometry structure of LUMO & HOMO orbitals for Apigenin and Luteolin compounds.

Table 9. Chemical structure, Chemical formula, and molar mass of Apigenin and Luteolin.

	Apigenin	**Luteolin**
Chemical structure	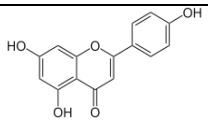	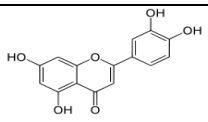
IUPAC name	5,7-Dihydroxy-2-(4-hydroxyphenyl)-4H-1-benzopyran-4-one	2-(3,4-Dihydroxyphenyl)- 5,7-dihydroxy-4-chromenone
Chemical formula	$C_{15}H_{10}O_5$	$C_{15}H_{10}O_6$
Molar mass	270.240 g·mol^{-1}	286.239 g·mol^{-1}

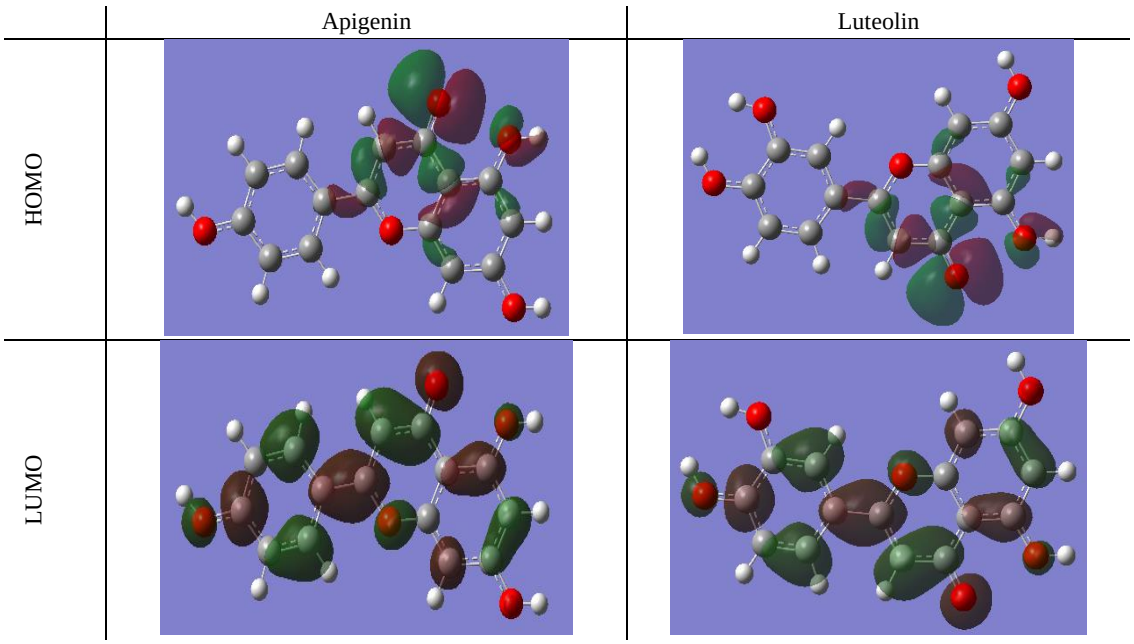

Figure 20. The optimum geometry structure and LUMO & HOMO orbitals for Apigenin and Luteolin compounds.

2.5.2. Dynamics simulations studies.

Figure 21 illustrates the suitable arranging to absorb AE constituents on the Fe (1 1 0) substrate. Table 11 shows the simulation of Monte Carlo resulting; distortion energies, total energy and solid adsorption. Total energy (substrate energy) is the totality of the energy of solid adsorption, molecules, and deformation energy. The substrate energy is taken as zero. In addition, the adsorption energy shows the gained or wanted energy when the comfortable adsorption of AE compounds takes place on the substrate. The rigid adsorption energy shows the gained or wanted energy when the uncomfortable adsorption of AE compounds has happened. It has occurred before the geometry optimization adsorption has occurred onto the substrate. It takes place before occurring the geometry optimization adsorption onto the substrate. The deformation energy is liberalized when the adsorption of AE compounds is restful on the substrate. The energy of substrate - adsorbate conformations (dEads / dNi) exhibits that one of the adsorbed compounds is taken away [69]. The results in Table 11 confirm that the examined AE shows high adsorption on the Zn surface.

Table 10 illustrates the quantum chemistry parameters (E_{LUMO}, E_{HOMO}, dipole moment (μ), and energy gap (ΔE)) for AE constituents. E_{HOMO} signifies the susceptibility of molecules to grant electrons to the d orbital of Zn, so molecules with high E_{HOMO} values have the potency to grant electrons to the metal surface. Negative E_{HOMO} values signalize physical adsorption rather than chemical one [63,64]. E_{LUMO} represents the capability of metal orbital to gain an electron, and its low value shows more capability for electrons accepting [65,66]. An inverse relationship between molecule reactivity and energy gap (ΔE) means that the smaller energy gap shows good corrosion inhibition because the ionization energy needed to eliminate the electron from the exterior orbit shell is low. The dipole moment (μ) represents the electrons distribution in the molecule, and it is a measure of the bond polarity [67]. A high μ indicates a strong dipole-dipole interaction with the Zn surface and tool up a good corrosion inhibition [68]. The quantum studies results confirm the experimental outcomes and show good inhibition of AE towards Zn corrosion.

Table 10. The quantum chemistry parameters (E_{LUMO}, E_{HOMO}, dipole moment (μ), and ΔE energy cavity) for AE constituents.

Comp.	E_{HOMO} (ev)	E_{LUMO} (ev)	ΔE (ev)	Dipole moment (Debye)
Apigenin	-5.505	-1.361	4.144	2.4448
Luteolin	-5.475	-1.348	4.127	7.1421

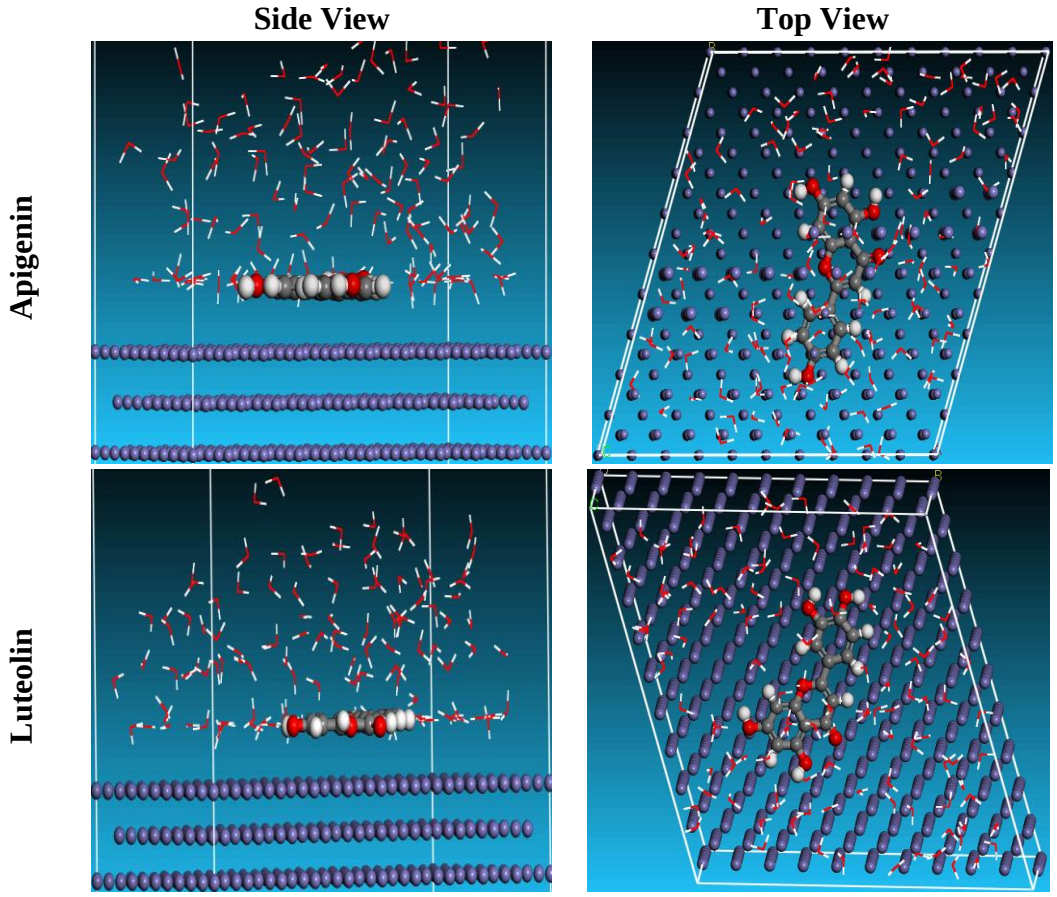

Figure 21. The suitable arranging to absorb AE constituents on the Fe (1 1 0) substrate.

Table 11. The simulation of Monte Carlo resulting; distortion energies, total energy, and solid adsorption.

Structures	Total Energy	Adsorption Energy	Rigid adsorption energy	Deformation Energy	Compound dEad/dNi	H_2O dEad/dNi
Fe (1 1 0)/ Apigenin/H_2O	-3228.3	-3154.7	-3312.5	157.8	-185.6	-8.3
Fe (1 1 0)/ Luteolin /H_2O	-3290.0	-3217.4	-3372.8	155.3	-200.1	-8.8

3.6. Inhibition mechanism analysis.

From the experiment results, the corrosion inhibition mechanism for Zn in the corrosive acid medium using AE can be explained from the view of adsorption. The main constituents of AE are Apigenin and Luteolin, which contain the oxygen atoms, hydroxyl groups, and three benzene rings in their structures. The adsorption process can be deemed as a mono exchange process in which the aqueous molecule (I) replaces several adsorbed water molecules (x) on the metal surface [70]:

$$I_{(aq)} + x\ H_2O_{(sur)} \rightarrow I_{(sur)} + x\ H_2O_{(aq)} \qquad (15)$$

The adsorption process can be affected by factors such as; charged surface, inhibitor structure, and the scuttled charge along the inhibitor molecule. The adsorption may be a

physisorption or chemisorption reaction. Generally, the physisorption process needs the existence of charged metal surfaces and charged molecules. At firstly, the anionic acid species were adsorbed on the Zn surface, making the surface negative. The protonated extract components can then be adsorbed on the surface. In the chemisorption process, the coordinate bond is formed between the extract and the metal surface by sharing or transferring the charge.

The existence of transition metal with unoccupied orbital and extracts with chemical constituents containing π-electrons and hetero atoms with a free lone pair of electrons (ex. N, O, S) is necessary and widely aid in the adsorption process [71].

4. Conclusions

AE showed good % IE reached 93.2 % at 300 ppm concentration. Adsorption of extract on Zn surface obeyed Langmuir isotherm. The inhibition action improved with increasing AE concentrations and decreased as the temperature increases. The adsorption of AE on Zn surface accords with Langmuir adsorption isotherm. Potentiodynamic polarization tests detected the extract worked as a mixed-type inhibitor with cathodic dominance. EIS tests displayed that a protective layer was formed on the Zn surface. This accords with the decrease in the C_{dl} value and the increase of the R_p with increasing AE concentration. The SEM/EDX, FTIR, and AFM examine presented a protective film of extract molecules above the Zn surface. The shape of UV spectroscopic indicated physisorption. The biological effect indicated that the number of Bacteria colonies for AE was lesser than the blank. Quantum mechanics and molecular dynamics simulation studies confirm the experimental results. Based on all outcomes of the applied techniques, it is attained that the employed extract works as a good corrosion inhibitor for zinc in acid solution, and its efficiency in the inhibition process raises with the increase in its concentration and decreases with the temperature rise.

Funding

This research received no external funding.

Acknowledgments

The authors are grateful to the Chemistry Department (especially corrosion laboratory), Faculty of Science, Mansoura University, for providing laboratory facilities for completing this work.

Conflicts of Interest

The authors declare no conflict of interest.

References

1. Garcia, G.; Cavallaro, L.; Broussalis, A.; Ferraro, G.; Martino, V.; De Torres, R.; Coussio, J.; Campos, R. Antiviral activity of Achyrocline flaccida Wein DC aqueous extract. *Phytotherapy Research* **1995**, *9*, 251-254, https://doi.org/10.1002/ptr.2650090404.
2. Manov, S.; Noli, F.; Lamazouere, A.M.; Aries, L. Surface treatment for zinc corrosion protection by a new organic chelating reagent. *Journal of Applied Electrochemistry* **1999**, *29*, 995-1003, https://doi.org/10.1023/A:1003585816876.
3. Wranglen, G. *An introduction to corrosion and protection of metals*; 1985.
4. Fouda, A.S.; Shalabi, K.; Nofal, A.M.; Elzekred, M.A. Methanol Extract of Rumex Vesicarius L. as Eco-Friendly Corrosion Inhibitor for Carbon Steel in Sulfuric Acid Solution. *Chemical Science Transactions* **2018**, *7*, 101-111, https://doi.org/10.7598/cst2018.1430.

5. Fouda, A.S.; Abdel Haleem, E. Berry Leaves Extract as Green Effective Corrosion Inhibitor for Cu in Nitric Acid Solutions. *Surface Engineering and Applied Electrochemistry* **2018**, *54*, 498-507, https://doi.org/10.3103/S1068375518050034.
6. Fouda, A.S.; Rashwan, S.M.; Darwish, M.M.K.; Arman, N.M. Corrosion inhibition of Zn in a 0.5 M HCl solution by Ailanthus altissima extract. *Portugaliae Electrochimica Acta* **2018**, *36*, 309-323, https://doi.org/10.4152/pea.201805309.
7. Elabbasy, H.M.; Fouda, A.S. Olive leaf as green corrosion inhibitor for C-steel in Sulfamic acid solution. *Green Chemistry Letters and Reviews* **2019**, *12*, 332-342, https://doi.org/10.1080/17518253.2019.1646812.
8. Fouda, A.S.; Elabbasy, H.M. Corrosion inhibition effect of methanol extract of nerium oleander on copper in nitric acid solutions. *Int. J. Electrochem. Sci.* **2019**, *14*, 6884-6901, https://doi.org/10.20964/2019.07.31.
9. Elabbasy, H.M. Investigation of Withania Somnifera Extract as Corrosion Inhibitor for Copper in Nitric Acid Solutions. *Int. J. Electrochem. Sci* **2019**, *14*, 5355-5372, https://doi.org/10.20964/2019.06.23.
10. Bahlakeh, G.; Ramezanzadeh, B.; Dehghani, A.; Ramezanzadeh, M. Novel cost-effective and high-performance green inhibitor based on aqueous Peganum harmala seed extract for mild steel corrosion in HCl solution: Detailed experimental and electronic/atomic level computational explorations. *J. Mol. Liq.* **2019**, *283*, 174-195, https://doi.org/10.1016/j.molliq.2019.03.086.
11. Dehghani, A.; Bahlakeh, G.; Ramezanzadeh, B.; Ramezanzadeh, M. Detailed macro-/micro-scale exploration of the excellent active corrosion inhibition of a novel environmentally friendly green inhibitor for carbon steel in acidic environments. *Journal of the Taiwan Institute of Chemical Engineers* **2019**, *100*, 239-261, https://doi.org/10.1016/j.jtice.2019.04.002.
12. Sanaei, Z.; Ramezanzadeh, M.; Bahlakeh, G.; Ramezanzadeh, B. Use of Rosa canina fruit extract as a green corrosion inhibitor for mild steel in 1M HCl solution: A complementary experimental, molecular dynamics and quantum mechanics investigation. *Journal of Industrial and Engineering Chemistry* **2019**, *69*, 18-31, https://doi.org/10.1016/j.jiec.2018.09.013.
13. Keramatinia, M.; Ramezanzadeh, B.; Mahdavian, M. Green production of bioactive components from herbal origins through one-pot oxidation/polymerization reactions and application as a corrosion inhibitor for mild steel in HCl solution. *Journal of the Taiwan Institute of Chemical Engineers* **2019**, *105*, 134-149, https://doi.org/10.1016/j.jtice.2019.10.005.
14. Asadi, N.; Ramezanzadeh, M.; Bahlakeh, G.; Ramezanzadeh, B. Utilizing Lemon Balm extract as an effective green corrosion inhibitor for mild steel in 1M HCl solution: A detailed experimental, molecular dynamics, Monte Carlo and quantum mechanics study. *Journal of the Taiwan Institute of Chemical Engineers* **2019**, *95*, 252-272, https://doi.org/10.1016/j.jtice.2018.07.011.
15. majd, M.T.; Ramezanzadeh, M.; Bahlakeh, G.; Ramezanzadeh, B. Probing molecular adsorption/interactions and anti-corrosion performance of poppy extract in acidic environments. *J. Mol. Liq.* **2020**, *304*, 112750, https://doi.org/10.1016/j.molliq.2020.112750.
16. Dehghani, A.; Bahlakeh, G.; Ramezanzadeh, B.; Ramezanzadeh, M. Aloysia citrodora leaves extract corrosion retardation effect on mild-steel in acidic solution: Molecular/atomic scales and electrochemical explorations. *J. Mol. Liq.* **2020**, *310*, 113221, https://doi.org/10.1016/j.molliq.2020.113221.
17. Dehghani, A.; Bahlakeh, G.; Ramezanzadeh, B.; Ramezanzadeh, M. Potential role of a novel green eco-friendly inhibitor in corrosion inhibition of mild steel in HCl solution: Detailed macro/micro-scale experimental and computational explorations. *Construction and Building Materials* **2020**, *245*, 118464, https://doi.org/10.1016/j.conbuildmat.2020.118464.
18. Ngouné, B.; Pengou, M.; Nouteza, A.M.; Nanseu-Njiki, C.P.; Ngameni, E. Performances of Alkaloid Extract from Rauvolfia macrophylla Stapf toward Corrosion Inhibition of C38 Steel in Acidic Media. *ACS Omega* **2019**, *4*, 9081-9091, https://doi.org/10.1021/acsomega.9b01076.
19. Putilova, I.N.; Balezin, S.A.e.; Barannik, V.P. *Metallic corrosion inhibitors*; Pergamon Press: 1960.
20. Shehata, O.S.; Korshed, L.A.; Attia, A. Green corrosion inhibitors, past, present, and future, corrosion inhibitors, principles and recent applications. *London: IntechOpen* **2017**, http://dx.doi.org/10.5772/intechopen.72753.
21. Rottenberg, A.; Zohary, D. The wild ancestry of the cultivated artichoke. *Genet. Resour. Crop Evol.* **1996**, *43*, 53-58, https://doi.org/10.1007/BF00126940.
22. Ladha, D.G.; Naik, D.U.; Shah, N.K. Investigation of Cumin (Cuminum Cyminum) extract as an eco-friendly green corrosion inhibitor for pure aluminium in acid medium. *Journal of Materials and Environmental Science* **2013**, *4*, 701-708, https://www.researchgate.net/publication/287707875.
23. Cesar, G. Plant Phenolics and Human Health–Biochemistry. *Nutrition and Pharmacology. Wiley* **2009**, *632*.

24. Bruneton, J. *Pharmacognosy, phytochemistry, medicinal plants*; Lavoisier publishing: 1995.
25. Adzet, T.; Puigmacia, M. High-performance liquid chromatography of caffeoylquinic acid derivatives of Cynara scolymus L. leaves. *J. Chromatogr.* **1985**, *348*, 447-453, https://doi.org/10.1016/S0021-9673(01)92486-0.
26. ASTM G 1-90, Standard practice for preparing, cleaning, and evaluating corrosion test specimens. 1999.
27. Talati, J.D.; Desai, M.N.; Shah, N.K. Ortho-, meta-, and para-aminophenol-N-salicylidenes as corrosion inhibitors of zinc in sulfuric acid. *Anti-Corrosion Methods and Materials* **2005**, *52*, 108-117, https://doi.org/10.1108/00035590510584825.
28. Guruprasad, A.M.; Sachin, H.P.; Swetha, G.A.; Prasanna, B.M. Adsorption and inhibitive properties of seroquel drug for the corrosion of zinc in 0.1 M hydrochloric acid solution. *International Journal of Industrial Chemistry* **2019**, *10*, 17-30, https://doi.org/10.1007/s40090-018-0168-x.
29. Abdel-Rehim, S.S.; Khaled, K.F.; Abd-Elshafi, N.S. Electrochemical frequency modulation as a new technique for monitoring corrosion inhibition of iron in acid media by new thiourea derivative. *Electrochim. Acta* **2006**, *51*, 3269-3277, https://doi.org/10.1016/j.electacta.2005.09.018.
30. Bosch, R.W.; Hubrecht, J.; Bogaerts, W.F.; Syrett, B.C. Electrochemical Frequency Modulation: A New Electrochemical Technique for Online Corrosion Monitoring. *Corrosion* **2001**, *57*, 60-70, https://doi.org/10.5006/1.3290331.
31. El-Etre, A.Y.; Abdallah, M. Natural honey as corrosion inhibitor for metals and alloys. II. C-steel in high saline water. *Corros. Sci.* **2000**, *42*, 731-738, https://doi.org/10.1016/S0010-938X(99)00106-7.
32. Kaczerewska, O.; Leiva-Garcia, R.; Akid, R.; Brycki, B.; Kowalczyk, I.; Pospieszny, T. Effectiveness of O-bridged cationic gemini surfactants as corrosion inhibitors for stainless steel in 3M HCl: Experimental and theoretical studies. *J. Mol. Liq.* **2018**, *249*, 1113-1124, https://doi.org/10.1016/j.molliq.2017.11.142.
33. Lgaz, H.; Salghi, R.; Subrahmanya Bhat, K.; Chaouiki, A.; Shubhalaxmi; Jodeh, S. Correlated experimental and theoretical study on inhibition behavior of novel quinoline derivatives for the corrosion of mild steel in hydrochloric acid solution. *J. Mol. Liq.* **2017**, *244*, 154-168, https://doi.org/10.1016/j.molliq.2017.08.121.
34. Ramesh Saliyan, V.; Adhikari, A.V. Inhibition of corrosion of mild steel in acid media by N′-benzylidene-3-(quinolin-4-ylthio)propanohydrazide. *Bull. Mater. Sci.* **2008**, *31*, 699-711, https://doi.org/10.1007/s12034-008-0111-4.
35. El-Aal, A.; Sliem, M.; Abdullah, A. Caprylamidopropyl Betaine as a highly efficient eco-friendly corrosion inhibitor for API X120 steel in 1 M H2SO4. *Egyptian Journal of Chemistry* **2020**, *63*, 759-776, https://doi.org/10.21608/ejchem.2019.13652.1844.
36. Abdul Rahiman, A.F.S.; Sethumanickam, S. Corrosion inhibition, adsorption and thermodynamic properties of poly(vinyl alcohol-cysteine) in molar HCl. *Arabian Journal of Chemistry* **2017**, *10*, S3358-S3366, https://doi.org/10.1016/j.arabjc.2014.01.016.
37. Döner, A.; Kardaş, G. N-Aminorhodanine as an effective corrosion inhibitor for mild steel in 0.5M H2SO4. *Corros. Sci.* **2011**, *53*, 4223-4232, https://doi.org/10.1016/j.corsci.2011.08.032.
38. Manaranche, C.; Hornberger, H. A proposal for the classification of dental alloys according to their resistance to corrosion. *Dent. Mater.* **2007**, *23*, 1428-1437, https://doi.org/10.1016/j.dental.2006.11.030.
39. Zeino, A.; Abdulazeez, I.; Khaled, M.; Jawich, M.W.; Obot, I.B. Mechanistic study of polyaspartic acid (PASP) as eco-friendly corrosion inhibitor on mild steel in 3% NaCl aerated solution. *J. Mol. Liq.* **2018**, *250*, 50-62, https://doi.org/10.1016/j.molliq.2017.11.160.
40. Guo, L.; Kaya, S.; Obot, I.B.; Zheng, X.; Qiang, Y. Toward understanding the anticorrosive mechanism of some thiourea derivatives for carbon steel corrosion: A combined DFT and molecular dynamics investigation. *J. Colloid Interface Sci.* **2017**, *506*, 478-485, https://doi.org/10.1016/j.jcis.2017.07.082.
41. El-Sayed Shehata, O. Effect of acetamide derivative and its Mn-complex as corrosion inhibitor for mild steel in sulphuric acid. *Egyptian Journal of Chemistry* **2017**, *60*, 243-259, https://doi.org/10.21608/ejchem.2017.674.1014.
42. Hamani, H.; Douadi, T.; Daoud, D.; Al-Noaimi, M.; Rikkouh, R.A.; Chafaa, S. 1-(4-Nitrophenylo-imino)-1-(phenylhydrazono)-propan-2-one as corrosion inhibitor for mild steel in 1M HCl solution: Weight loss, electrochemical, thermodynamic and quantum chemical studies. *J. Electroanal. Chem.* **2017**, *801*, 425-438, https://doi.org/10.1016/j.jelechem.2017.08.031.
43. Laamari, M.R.; Benzakour, J.; Berrekhis, F.; Derja, A.; Villemin, D. Adsorption and corrosion inhibition of carbon steel in hydrochloric acid medium by hexamethylenediamine tetra(methylene phosphonic acid). *Arabian Journal of Chemistry* **2016**, *9*, S245-S251, https://doi.org/10.1016/j.arabjc.2011.03.018.

44. Chauhan, D.S.; Ansari, K.R.; Sorour, A.A.; Quraishi, M.A.; Lgaz, H.; Salghi, R. Thiosemicarbazide and thiocarbohydrazide functionalized chitosan as ecofriendly corrosion inhibitors for carbon steel in hydrochloric acid solution. *Int. J. Biol. Macromol.* **2018**, *107*, 1747-1757, https://doi.org/10.1016/j.ijbiomac.2017.10.050.
45. Salhi, A.; Tighadouini, S.; El-Massaoudi, M.; Elbelghiti, M.; Bouyanzer, A.; Radi, S.; El Barkany, S.; Bentiss, F.; Zarrouk, A. Keto-enol heterocycles as new compounds of corrosion inhibitors for carbon steel in 1M HCl: Weight loss, electrochemical and quantum chemical investigation. *J. Mol. Liq.* **2017**, *248*, 340-349, https://doi.org/10.1016/j.molliq.2017.10.040.
46. Mohan, R.; Joseph, A. Corrosion protection of mild steel in hydrochloric acid up to 313K using propyl benzimidazole: Electroanalytical, adsorption and quantum chemical studies. *Egyptian Journal of Petroleum* **2018**, *27*, 11-20, https://doi.org/10.1016/j.ejpe.2016.12.003.
47. Benabdellah, M.; Tounsi, A.; Khaled, K.F.; Hammouti, B. Thermodynamic, chemical and electrochemical investigations of 2-mercapto benzimidazole as corrosion inhibitor for mild steel in hydrochloric acid solutions. *Arabian Journal of Chemistry* **2011**, *4*, 17-24, https://doi.org/10.1016/j.arabjc.2010.06.010.
48. Reis, F.M.; de Melo, H.G.; Costa, I. EIS investigation on Al 5052 alloy surface preparation for self-assembling monolayer. *Electrochim. Acta* **2006**, *51*, 1780-1788, https://doi.org/10.1016/j.electacta.2005.02.118.
49. Solmaz, R.; Kardaş, G.; Çulha, M.; Yazıcı, B.; Erbil, M. Investigation of adsorption and inhibitive effect of 2-mercaptothiazoline on corrosion of mild steel in hydrochloric acid media. *Electrochim. Acta* **2008**, *53*, 5941-5952, https://doi.org/10.1016/j.electacta.2008.03.055.
50. Tao, Z. H.; Zhang, S. T.; Li, W. H.; Hou, B. R. Corrosion inhibition of mild steel in acidic solution by some oxo-triazole derivatives. *Corros. Sci.* **2009**, *51*, 2588-2595, https://doi.org/10.1016/j.corsci.2009.06.042.
51. Yousefi, A.; Javadian, S.; Dalir, N.; Kakemam, J.; Akbari, J. Imidazolium-based ionic liquids as modulators of corrosion inhibition of SDS on mild steel in hydrochloric acid solutions: experimental and theoretical studies. *RSC Advances* **2015**, *5*, 11697-11713, https://doi.org/10.1039/C4RA10995C.
52. Volpi, E.; Foiadelli, C.; Trasatti, S.; Koleva, D.A. Development of Smart Corrosion Inhibitors for Reinforced Concrete Structures Exposed to a Microbial Environment. *Ind. Eng. Chem. Res.* **2017**, *56*, 5778-5794, https://doi.org/10.1021/acs.iecr.7b00127.
53. Zheng, X.; Gong, M.; Li, Q.; Guo, L. Corrosion inhibition of mild steel in sulfuric acid solution by loquat (Eriobotrya japonica Lindl.) leaves extract. *Sci. Rep.* **2018**, *8*, 9140, https://doi.org/10.1038/s41598-018-27257-9.
54. Shalabi, K.; Abdallah, Y.; Hassan, H.; Fouda, A. Effects of Arctostaphylos uva-ursi Extract as Green Corrosion Inhibitor for Cu10Ni Alloy in 1 M HNO3. *International journal of electrochemical science* **2014**, *9*, 5073, https://www.researchgate.net/publication/263274403.
55. Fouda, A.; Shalabi, K.; Elewady, G.; Emrayed, H. Chalcone Derivatives as Corrosion Inhibitors for Carbon Steel in 1 M HCl Solutions. *International journal of electrochemical science* **2014**, *9*, 7038-7058, https://www.researchgate.net/publication/266262341.
56. Rajendran, S.; Thangavelu, C.; Annamalai, G. Inhibition of corrosion of aluminium in alkaline medium by succinic acid in conjunction with zinc sulphate and diethylene triamine penta (Methylene phosphonic acid). *J. Chem. Pharm. Res.* **2012**, *4*, 4836-4844, https://www.researchgate.net/publication/286571211.
57. Mu, G.; Li, X.; Liu, G. Synergistic inhibition between tween 60 and NaCl on the corrosion of cold rolled steel in 0.5M sulfuric acid. *Corros. Sci.* **2005**, *47*, 1932-1952, https://doi.org/10.1016/j.corsci.2004.09.020.
58. Wang, B.; Du, M.; Zhang, J.; Gao, C.J. Electrochemical and surface analysis studies on corrosion inhibition of Q235 steel by imidazoline derivative against CO2 corrosion. *Corros. Sci.* **2011**, *53*, 353-361, https://doi.org/10.1016/j.corsci.2010.09.042.
59. Chugh, B.; Singh, A.K.; Thakur, S.; Pani, B.; Lgaz, H.; Chung, I.-M.; Jha, R.; Ebenso, E.E. Comparative Investigation of Corrosion-Mitigating Behavior of Thiadiazole-Derived Bis-Schiff Bases for Mild Steel in Acid Medium: Experimental, Theoretical, and Surface Study. *ACS Omega* **2020**, *5*, 13503-13520, https://doi.org/10.1021/acsomega.9b04274.
60. Obi-Egbedi, N.O.; Obot, I.B. Xanthione: A new and effective corrosion inhibitor for mild steel in sulphuric acid solution. *Arabian Journal of Chemistry* **2013**, *6*, 211-223, https://doi.org/10.1016/j.arabjc.2010.10.004.
61. Ituen, E.; Akaranta, O.; James, A. Green anticorrosive oilfield chemicals from 5-hydroxytryptophan and synergistic additives for X80 steel surface protection in acidic well treatment fluids. *J. Mol. Liq.* **2016**, *224*, 408-419, https://doi.org/10.1016/j.molliq.2016.10.024.

62. Goel, R.; Siddiqi, W.A.; Ahmed, B.; Khan, M.S.; Chaubey, V.M. Synthesis characterization and corrosion inhibition efficiency of N-C2 {(2E)-2-[4-(dimethylamino) benzylidene] hydrazinyl} 2-oxo ethyl benzamide on mild steel. *Desalination* **2010**, *263*, 45-57, https://doi.org/10.1016/j.desal.2010.06.033.
63. Aytaç, A.; Bilgiç, S.; Gece, G.; Ancın, N.; Öztaş, S.G. Experimental and theoretical study of the inhibition effects of some Schiff bases as corrosion inhibitors of aluminium in HCl. *Mater. Corros.* **2012**, *63*, 729-734, https://doi.org/10.1002/maco.201106241.
64. Allam, N.K. Thermodynamic and quantum chemistry characterization of the adsorption of triazole derivatives during Muntz corrosion in acidic and neutral solutions. *Appl. Surf. Sci.* **2007**, *253*, 4570-4577, https://doi.org/10.1016/j.apsusc.2006.10.008.
65. Santos, A.d.M.; Almeida, T.F.d.; Cotting, F.; Aoki, I.V.; Melo, H.G.d.; Capelossi, V.R. Evaluation of castor bark powder as a corrosion inhibitor for carbon steel in acidic media. *Materials Research* **2017**, *20*, 492-505, https://doi.org/10.1590/1980-/5373-MR-2016-0963.
66. Idouhli, R.; N'Ait Ousidi, A.; Koumya, Y.; Abouelfida, A.; Benyaich, A.; Auhmani, A.; Ait Itto, M.Y. Electrochemical Studies of Monoterpenic Thiosemicarbazones as Corrosion Inhibitor for Steel in 1 M HCl. *International Journal of Corrosion* **2018**, *2018*, 9212705, https://doi.org/10.1155/2018/9212705.
67. Obot, I.B.; Obi-Egbedi, N.O. Indeno-1-one [2,3-b]quinoxaline as an effective inhibitor for the corrosion of mild steel in 0.5M H2SO4 solution. *Mater. Chem. Phys.* **2010**, *122*, 325-328, https://doi.org/10.1016/j.matchemphys.2010.03.037.
68. Mert, B.D.; Erman Mert, M.; Kardaş, G.; Yazıcı, B. Experimental and theoretical investigation of 3-amino-1,2,4-triazole-5-thiol as a corrosion inhibitor for carbon steel in HCl medium. *Corros. Sci.* **2011**, *53*, 4265-4272, https://doi.org/10.1016/j.corsci.2011.08.038.
69. Roque, J.M.; Pandiyan, T.; Cruz, J.; García-Ochoa, E. DFT and electrochemical studies of tris(benzimidazole-2-ylmethyl)amine as an efficient corrosion inhibitor for carbon steel surface. *Corros. Sci.* **2008**, *50*, 614-624, https://doi.org/10.1016/j.corsci.2007.11.012.
70. Fouda, A.E.-A.S.; Farahat, M.M.; Abdallah, M. Cephalosporin antibiotics as new corrosion inhibitors for nickel in HCl solution. *Res. Chem. Intermed.* **2014**, *40*, 1249-1266, https://doi.org/10.1007/s11164-013-1036-0.
71. Abd, E.-A.F.S.; Ali, A.H. Egy-dronate drug as promising corrosion inhibitor of C-steel in aqueous medium. *Zaštita materijala* **2018**, *59*, 126-140, https://doi.org/10.5937/ZasMat1801128F.